ELSEVIER

Chemical Engineering Science 60 (2005) 213–218

Chemical Engineering Science

www.elsevier.com/locate/ces

A generalized approach to model oxygen transfer in bioreactors using population balances and computational fluid dynamics

Kumar M. Dhanasekharan*, Jay Sanyal, Anupam Jain, Ahmad Haidari

Fluent Inc., 10 Cavendish Court, NH 03766, Lebanon

Received 9 June 2003; received in revised form 18 May 2004; accepted 28 July 2004
Available online 23 September 2004

Abstract

In many biological processes, increasing the rate of transport of a limiting nutrient can enhance the rate of product formation. In aerobic fermentation systems, the rate of oxygen transfer to the cells is usually the limiting factor. A key factor that influences oxygen transfer is bubble size distribution. The bubble sizes dictate the available interfacial area for gas–liquid mass transfer. Scale-up and design of bioreactors must meet oxygen transfer requirements while maintaining low shear rates and a controlled flow pattern. This is the motivation for the current work that captures multiphase hydrodynamics and simultaneously predicts the bubble size distribution.

Bubbles break up and coalesce due to interactions with turbulent eddies, giving rise to a distribution of bubble sizes. These effects are included in the modeling approach by solving a population balance model with bubble breakage and coalescence. The population balance model was coupled to multiphase flow equations and solved using a commercial computational fluid mechanics code FLUENT 6. Gas holdup and volumetric mass transfer coefficients were predicted for different superficial velocities and compared to the experimental results of Kawase and Hashimoto (1996). The modeling results showed good agreement with experiment.

Keywords: Airlift; Bioreactor; Gas holdup; Mass transfer; Loop reactor; Bubble column reactor

1. Introduction

Bioreactors have the potential to become integral to the development of high-value products and the replacement of existing chemical-based commodity processes. The most common type of aerobic bioreactor in use today is the stirred tank reactor with baffles and agitators and other internals designed for specific applications. For certain industrial scale applications however, airlift reactors provide a simple design with no moving parts and generate lower shear rates for shear-sensitive microorganisms. Additionally, increased mass transfer due to enhanced oxygen solubility at higher pressures can be achieved in tall airlift reactor vessels. The current work focuses on airlift bioreactors.

The rate of oxygen transfer to the cells is one of the limiting factors in product formation. It is known that increasing the rate of oxygen transfer can enhance the rate of product formation. Gas holdup and the liquid volumetric mass transfer coefficient are commonly used to characterize oxygen transfer. Oxygen transfer is strongly influenced by the hydrodynamics of bubbles. Several researchers have studied the hydrodynamics and mass transfer in bioreactors (Pandit and Joshi, 1986; Beenackers and Swaaji, 1993; Veerlan and Tramper, 1987; Mao et al., 1992; Kochbeck et al., 1992; Douek et al., 1994). In recent years, computational fluid mechanics (CFD) tools have been used for studying the hydrodynamics of airlift reactors using bubbly two-phase flow models. Cockx et al. (1997) proposed a model based on one-dimensional (1D) two-fluid mass and momentum balances where closure relations for the slip velocity of the gas bubbles, friction factors and singular pressure drop coefficients are obtained from three-dimensional CFD

* Corresponding author. Tel.: +961-603-643-2600x323; fax: +961-603-643-3967.
E-mail address: kd@fluent.com (K.M. Dhanasekharan).

0009-2509/$ - see front matter © 2004 Elsevier Ltd. All rights reserved.
doi:10.1016/j.ces.2004.07.118

simulations. Sokolichin and Eigenberger (1994) reviewed the modeling of gas–liquid flow in bubble columns and loop reactors. Results obtained with dynamic multidimensional two-fluid models were compared with respective steady-state simulations. Most literature do not account for the dynamic breakage and coalescence of bubbles. The bubble size distribution is important since the interfacial area is the key parameter that controls the oxygen transfer rate. Mudde and Van Den Akker (2001) conducted 2D and 3D numerical simulations of an internal airlift loop reactor based on the two-fluid model. The results were compared with LDA data and the 2D results showed deviation from experiments at higher superficial velocities, while the 3D results seemed to compare favorably. Burris et al. (2002) developed a simple model that predicts oxygen transfer based on discrete-bubble principles. They did not model the detailed hydrodynamics of the airlift reactor. Bezzo et al. (2003) demonstrated a multizonal/computational fluid dynamics (CFD) modeling approach to study the interaction between fluid-flow and biological reactions. More recently, Wang et al. (2004) studied the influence of the superficial gas velocity and solid holdup on the global gas holdup and radial profiles of the suspension circulation velocity in the downer and of gas holdup, bubble size, and bubble rise velocity in the riser using fiber optic probe and ultrasound Doppler velocimetry. Hristov et al. (2004) developed a simplified CFD model for three-dimensional analysis of fluid-flow and bioreactions in stirred tank reactors with novel impellers. The network-of-zones model previously developed by the authors for Rushton turbine was modified and the results indicated that the oxygen levels predicted is completely different from that obtained by an oversimplified plug (gas)-backmixed-(liquid) bioreactor model.

The current work builds on existing knowledge by developing a full CFD model that is coupled with bubble dynamics. The work demonstrates a generalized approach to couple bubble dynamics of breakage and coalescence with fluid-flow equations for multiphase flows. With this approach there is no need for correlations that apply only for certain geometric configurations and flow conditions. Novel bioreactor designs can be greatly improved by understanding the spatial and temporal variations of bubble volume and number distribution throughout the bioreactor using this method. The numerical solutions are validated with experimental data from Kawase and Hashimoto (1996).

Kawase and Hashimoto (1996) conducted extensive experimental studies with a laboratory external-loop airlift reactor for both Newtonian and non-Newtonian media in the presence and absence of solids. They also proposed correlations for predicting gas holdup and mass transfer coefficients. In the current work, we conducted numerical simulations for Newtonian media without solids and compared against equivalent experimental results.

2. Modeling approach

The air–water system is considered as a two-phase flow using a full multi-fluid Eulerian model. In this approach mass and momentum balance equations are solved for each phase. The coupling between phases is achieved through interphase exchange terms. The mass and momentum balance equations can be written as

$$\frac{\partial}{\partial t}\alpha_L\rho_L + \nabla\cdot(\alpha_L\rho_L\vec{u}_L) = 0, \tag{1}$$

$$\frac{\partial}{\partial t}\alpha_G\rho_G + \nabla\cdot(\alpha_G\rho_G\vec{u}_G) = 0, \tag{2}$$

$$\begin{aligned}\frac{\partial}{\partial t}(\alpha_L\rho_L\vec{u}_L) + \nabla\cdot(\alpha_L\rho_L\vec{u}_L\vec{u}_L)\\ = -\alpha_L\nabla P + \nabla\cdot\bar{\bar{\tau}}_L + K_{GL}(\vec{u}_G - \vec{u}_L)\\ + \alpha_L\rho_L\vec{\mathbf{g}},\end{aligned} \tag{3}$$

$$\begin{aligned}\frac{\partial}{\partial t}(\alpha_G\rho_G\vec{u}_G) + \nabla\cdot(\alpha_G\rho_G\vec{u}_G\vec{u}_G)\\ = -\alpha_G\nabla P + \nabla\cdot\bar{\bar{\tau}}_G + K_{LG}(\vec{u}_L - \vec{u}_G)\\ + \alpha_G\rho_G\vec{\mathbf{g}}.\end{aligned} \tag{4}$$

The drag coefficient $K_{GL} = K_{LG}$ is taken from Schiller and Naumann (1933). The turbulence was modeled using standard $k-\boldsymbol{\varepsilon}$ model (Launder and Spalding, 1972) suitably extended to multiphase flows (Simonin). The equations describing this model are

$$\begin{aligned}\frac{\partial}{\partial t}\boldsymbol{\rho}_m k + \nabla\cdot\boldsymbol{\rho}_m\bar{u}_m k\\ = \nabla\cdot\left(\frac{\boldsymbol{\mu}_m^t}{\boldsymbol{\sigma}_k}\nabla k\right) + G_{k,m} - \boldsymbol{\rho}_m\boldsymbol{\varepsilon},\end{aligned} \tag{5}$$

$$\begin{aligned}\frac{\partial}{\partial t}\boldsymbol{\rho}_m\boldsymbol{\varepsilon} + \nabla\cdot\boldsymbol{\rho}_m\bar{u}_m\boldsymbol{\varepsilon}\\ = \nabla\cdot\left(\frac{\boldsymbol{\mu}_m^t}{\boldsymbol{\sigma}_\varepsilon}\nabla\boldsymbol{\varepsilon}\right) + \frac{\boldsymbol{\varepsilon}}{k}(C_{1\varepsilon}G_{k,m} - C_{2\varepsilon}\boldsymbol{\rho}_m\boldsymbol{\varepsilon}).\end{aligned} \tag{6}$$

The mixture properties in Eqs. (5) and (6) are given by

$$\begin{aligned}\rho_m &= \alpha_G\rho_G + \alpha_L\rho_L;\\ \vec{u}_m &= \frac{\alpha_G\rho_G\vec{u}_G + \alpha_L\rho_L\vec{u}_L}{\rho_m}.\end{aligned} \tag{7}$$

The turbulent viscosity $\boldsymbol{\mu}_{t,m}$ is computed from

$$\boldsymbol{\mu}_m^t = \boldsymbol{\rho}_m C_{\boldsymbol{\mu}}\frac{k^2}{\boldsymbol{\varepsilon}} \tag{8}$$

and the production of turbulence kinetic energy, $G_{k,m}$, is computed from

$$G_{k,m} = \mu_m^t(\nabla\vec{u}_m + (\nabla\vec{u}_m)^{\mathrm{T}}) : \nabla\vec{u}_m. \tag{9}$$

The constants C_μ, etc. were obtained from Launder and Spalding (1972).

The gas phase is assumed to be composed of 9 discrete bubble sizes and a discretized population balance equation is solved for the bubble number density along with birth and death terms due to breakup and coalescence. The equation for the ith bubble class fraction f_i is written as

$$\frac{\partial \boldsymbol{\alpha}_G \boldsymbol{\rho}_G f_i}{\partial t} + \nabla \cdot (\boldsymbol{\alpha}_G \boldsymbol{\rho}_G \bar{u}_G) f_i = S_i, \tag{10}$$

$$S_i = B_{\text{Breakup}} - D_{\text{Breakup}} + B_{\text{Coalescence}} - D_{\text{Coalescence}}, \tag{11}$$

where f_i is defined as the ratio of total volume of bubbles of class i to the total volume of bubbles of all classes. These functions are expressed as

$$B_{\text{breakup}}(v; \mathbf{x}, t) = \int_{v_{\max}-v}^{v_{\max}} \boldsymbol{\Omega}_B(v', v) n(v'; \mathbf{x}, t)\, \mathrm{d}v', \tag{12}$$

$$D_{\text{breakup}}(v; \mathbf{x}, t) = n(v; \mathbf{x}, t) \int_0^{v/2} \frac{\boldsymbol{\Omega}_B(v, v')}{v}\, \mathrm{d}v', \tag{13}$$

$$B_{\text{coalescence}}(v; \mathbf{x}, t) = \int_0^{v/2} P_c(v - v', v).\boldsymbol{\omega}(v - v', v) \times n(v - v'; \mathbf{x}, t) n(v'; \mathbf{x}, t)\, \mathrm{d}v', \tag{14}$$

$$D_{\text{coalesence}}(v; \mathbf{x}, t) = \int_0^{v_{\max}-v} P_c(v, v').\boldsymbol{\omega}(v, v') \times n(v; \mathbf{x}, t) n(v'; \mathbf{x}, t)\, \mathrm{d}v'. \tag{15}$$

The bubble breakup and coalescence kernels appearing in the integrals above are described below.

Bubble breakup is analyzed in terms of bubble interactions with turbulent eddies. The turbulent eddies increase the surface energy of the bubbles through deformation. Breakup occurs if the increase in surface energy reaches a critical value. A binary breakage is assumed. The kernel contains no adjustable parameters. The breakup rate of particles of size v into particle sizes of vf_{BV} and $v\,(1 - f_{BV})$ is given as (Luo, 1993)

$$\frac{\Omega_B(v : vf_{BV})}{(1 - \boldsymbol{\varepsilon}_d) n} = c_4 \left(\frac{\boldsymbol{\varepsilon}}{d^2}\right)^{1/3} \int_{\xi_{\min}}^{1} \frac{(1 + \xi)^2}{\xi^{11/3}} \times \exp\left(-\frac{12 c_f \sigma}{\beta \rho_L \boldsymbol{\varepsilon}^{2/3} d^{5/3} \xi^{11/3}}\right) \mathrm{d}\xi, \tag{16}$$

where

$$c_f = f_{BV}^{2/3} + (1 - f_{BV})^{2/3} - 1. \tag{17}$$

Bubble coalescence is modeled by considering bubble collisions due to turbulence, buoyancy and laminar shear. The coalescence rate is given as a product of collision frequency and coalescence probability. The coalescence probability of bubbles of sizes v_i and v_j is expressed as (Luo, 1993)

$$P_C(v_i, v_j) = \exp\left(-c_1 \rho_L d_i (v_i^2 + v_j^2)^{1/2} \times \frac{[0.75(1 + \xi_{ij}^2)(1 + \xi_{ij}^3)]^{1/2}}{\sigma(\rho_G/\rho_L + \gamma)^{1/2}(1 + \xi_{ij})^3}\right), \tag{18}$$

where

$$\gamma = \frac{12 c_f \boldsymbol{\sigma}}{\boldsymbol{\rho}_L d_i \boldsymbol{\beta} \boldsymbol{\varepsilon}^{2/3}}. \tag{19}$$

The collision frequency is given as (Luo, 1993)

$$\omega_c(v_i, v_j) = (\pi/4)(d_i + d_j)^2 n_i n_j (v_i^2 + v_j^2)^{1/2}. \tag{20}$$

The coupling between bubble breakup and coalescence and CFD is achieved through the dynamic drag term based on the sauter mean diameter d_{32}.

Eqs. (1)–(4) and (10) were solved numerically with a commercial CFD code FLUENT 6 that is based on the finite volume method.

3. Results and discussion

The computational grid is shown in Fig. 1. The flow geometry was discretized into 23,000 hexahedral cells. Due to symmetry only one-half of the reactor geometry was modeled. The dimensions of the riser diameter and the downcomer diameter are 0.07 and 0.155 m, respectively. The volume of the reactor is 0.023 m^3. For this geometry, five CFD runs were conducted for superficial gas velocities of 0.01, 0.02, 0.03, 0.04 and 0.05 m/s. Riser Gas holdup (ϕgr) was calculated as the ratio of the volume increase of gas in the riser section divided by the initial liquid volume in the riser. The volumetric mass transfer coefficient was calculated as the product of liquid-phase mass transfer coefficient (K_L) and the specific surface area a.

K_L is obtained from the basis of Higbie's penetration theory as

$$K_L = \frac{2}{\sqrt{\boldsymbol{\pi}}} \sqrt{D} \left\{\frac{\boldsymbol{\varepsilon}_L \boldsymbol{\rho}_L}{\boldsymbol{\mu}_L}\right\}^{0.25}, \tag{21}$$

where $\boldsymbol{\varepsilon}_L$ is the water turbulent dissipation rate that is predicted from the CFD simulation. The interfacial area is also directly obtained from the predicted bubble size distribution as

$$a = \sum_i \frac{6\boldsymbol{\alpha}_i}{d_i}. \tag{22}$$

Fig. 2 shows contours of air volume fraction of 0.1 for a superficial velocity of 0.03 m/s. Fig. 3 shows contours of air volume fraction along the symmetry plane for the same conditions. From Figs. 2 and 3 it can be seen that most of the air rises through the riser section and leaves the domain. However, a small pocket of air is seen to be trapped in the

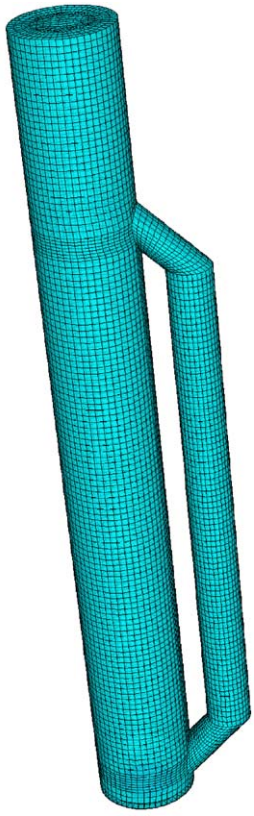

Fig. 1. Airlift reactor geometry and experimental conditions taken from Kawase and Hashimoto (1996). Finite volume mesh with 23,000 hexahedral cells for 180° of flow geometry.

Fig. 2. Isovalues of volume fraction of air $= 0.1$ in the airlift reactor showing the rising air plume for superficial velocity of 0.03 m/s.

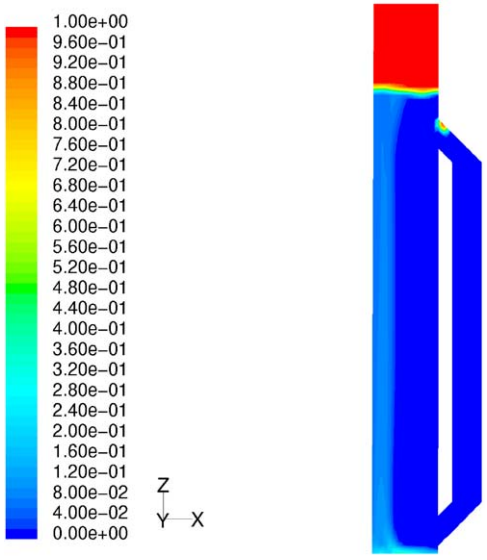

Fig. 3. Contours of volume fraction of air along symmetry plane for superficial velocity of 0.03 m/s.

bend section of the downcomer. The air bubbles generally tend to follow the liquid velocity vectors and consequently get trapped at the entry to downcomer where the liquid flow separates. A closer look at the liquid velocities clearly reveals this recirculatory flow behavior in Fig. 4. A large area of recirculatory liquid flow can also be observed in the riser section. This explains why the buoyant air is pushed towards the side away from the downcomer as seen in Fig. 3. In a well-designed external loop bioreactor, we expect to see the flow rising in the riser section and flow moving downwards in the downcomer section. However, there is an optimum ratio of downcomer diameter to riser diameter that will exhibit this desired behavior. In the current case, this ratio is not optimized for the current superficial velocities and hence an undesirable recirculation is noticed in the riser section. Fig. 5 shows the mean diameter distribution of the bubbles. The larger bubbles are seen to rise with the liquid in the riser section. The smaller bubbles tend to be carried downwards by the liquid circulation in both the riser and downcomer sections. Fig. 6 shows the comparison of our predictions of riser gas holdup with the experimental data of Kawase and Hashimoto (1996). The gas holdup values are well predicted for smaller superficial velocities compared to the values at larger superficial velocities. However, the overall predictions are in the same order of magnitude and the maximum error is only about 13%. Fig. 7 shows the comparison of our predictions of volumetric mass transfer coefficient with experimental data of Kawase and Hashimoto (1996). The CFD simulations over predict the mass transfer data by about 25% in the worst case. Typical CFD simulations can capture the

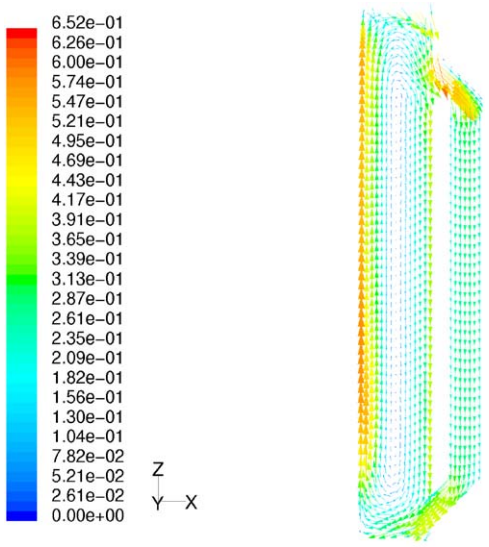

Fig. 4. Velocity vectors of water in the airlift reactor along symmetry plane showing circulation patterns for superficial velocity of 0.03 m/s.

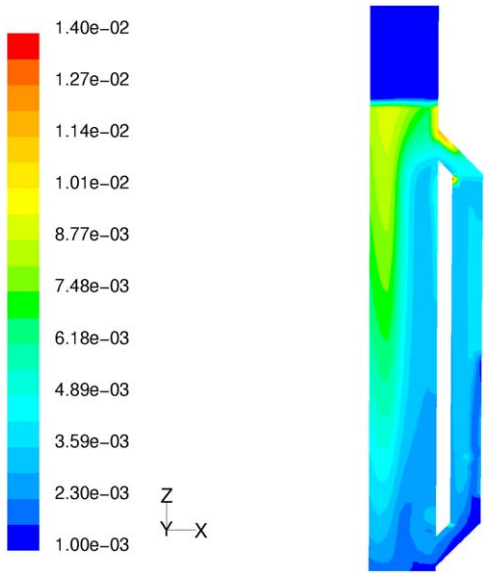

Fig. 5. Contours of d_{32} in mm along symmetry plane for superficial velocity of 0.03 m/s.

gas holdup correctly, but the prediction of mass transfer coefficient is more difficult due to limitations in capturing the bubble number density distribution accurately. The accuracy can be improved by refining the discretization of the population balance equation for bubble number density at the cost of increased computational time. The assumptions of the breakup coalescence models may also have to be revisited and modified. Nevertheless, the current results indicate good comparison toexperimental data for both gas holdup and volumetric mass transfer coefficient.

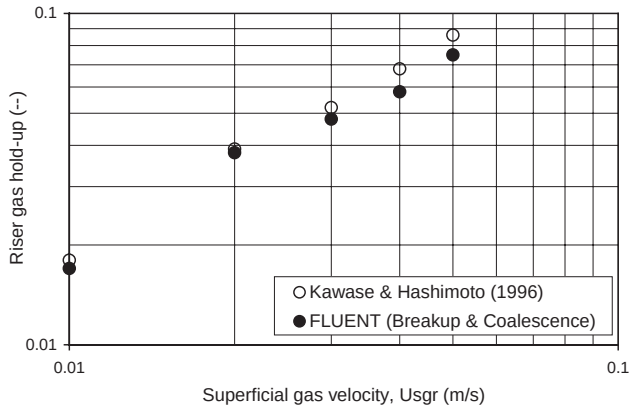

Fig. 6. Comparison of CFD predictions of gas hold-up with experimental results of Kawase and Hashimoto (1996).

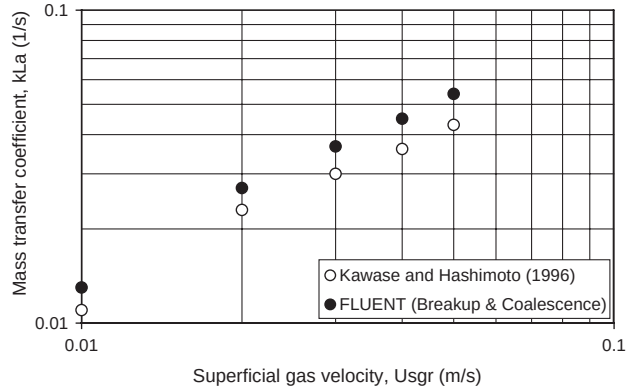

Fig. 7. Comparison of CFD predictions of volumetric mass transfer coefficient with experimental results of Kawase and Hashimoto (1996).

4. Conclusions

A generalized approach to predict oxygen transfer for bioreactors has been developed. The model predictions show good agreement with experimental data. The developed methodology can be applied to stirred tank and airlift bioreactors at different scales of operation. Thus the approach can be used for scale-up of bioprocesses. The model can be improved further by solving for more number of discrete bubble size equations to resolve the bubble size distribution more accurately. Additionally, different bubble breakup and coalescence mechanisms may have to be investigated to account for non-Newtonian media and presence of surfactants and impurities.

Notation

$C_{1\varepsilon}$	constant, 1.44
$C_{2\varepsilon}$	constant, 1.92
C_{μ}	constant, 0.09

C_4 constant, 0.923
d_i bubble diameter, m
f_i fraction of bubbles of class i
g gravity $= 9.81\,\mathrm{m/s^2}$
k turbulent kinetic energy, $\mathrm{m^2/s^2}$
n_i bubble number density of class i
P pressure, Pa
u_i velocity of phase i, m/s

Greek letters

α_i volume fraction of phase i
β constant, 2.41
ε turbulent dissipation rate, $\mathrm{m^2/s^3}$
ξ_{ij} size ratio of bubbles
ρ_i density of phase i, $\mathrm{kg/m^3}$
σ surface tension, N/m
τ_i stress tensor of phase i, $\mathrm{N/m^2}$

Subscripts

G gas phase
L liquid phase

References

Beenackers, A.A.C.M., Van Swaaji, W.P.M., 1993. Mass transfer in gas–liquid slurry reactors. Chemical Engineering Science 48, 3109–3139.

Bezzo, F., Macchietto, S., Pantelides, C.C., 2003. General hybrid multizonal/ CFD approach for bioreactor modeling. A.I.Ch.E. Journal 49, 2133–2148.

Burris, V.L., McGinnis, D.F., Little, J.C., 2002. Predicting oxygen transfer and water flow rate in airlift reactors. Water Research 36, 4605–4615.

Cockx, A., Line, A., Roustan, M., Do-Quang, Z., Lazarova, V., 1997. Numerical simulation and physical modeling of the hydrodynamics in an air-lift internal loop reactor. Chemical Engineering Science 52 (21/22), 3787–3793.

Douek, R.S., Livingston, A.G., Johansson, A.C., Hewitt, G.F., 1994. Hydrodynamics of an external-loop three phase airlift reactor. Chemical Engineering Science 49, 3719–3737.

Hristov, H.V., Mann, R., Lossev, V., Vlaev, S.D., 2004. A simplified CFD for three-dimensional analysis of fluid mixing, mass transfer and bioreaction in a fermenter equipped with triple novel geometry impellers. Food and Bioproducts Processing 82, 21–34.

Kawase, Y., Hashimoto, N., 1996. Gas hold-up and oxygen transfer in three-phase external loop airlift bioreactors: non-Newtonian fermentation broths. Journal of Chemical Technology and Biotechnology 65, 325–334.

Kochbeck, B., Lindert, M., Hempel, D.C., 1992. Hydrodynamics and local parameters in three-phase flow in airlift loop reactors of different scale. Chemical Engineering Science 47, 3443–3450.

Launder, B.E., Spalding, D.B., 1972. Lectures in Mathematical Models of Turbulence, Academic Press, London, UK.

Luo, H., 1993. Coalescence, breakup and circulation in bubble column reactors. Ph.D. Thesis, Trondheim, Norway.

Mao, H.H., Chisti, Y., Moo-Young, M., 1992. Multiphase hydrodynamics and solid–liquid mass transport in an external-loop airlift reactor—a comparative study. Chemical Engineering Communications 113, 1–13.

Mudde, R.F., Van Den Akker, H.E.A., 2001. 2D and 3D simulations of an internal airlift loop reactor on the basis of a two-fluid model. Chemical Engineering Science 56, 6351–6358.

Pandit, A.B., Joshi, J.B., 1986. Mass and heat transfer characteristics of three-phase sparged reactors. Chemical Engineering Research and Design 64, 125–157.

Schiller, L., Naumann, Z., 1933. A drag coefficient correlation. VDI-Zeitschrift 77, 318–320.

Sokolichin, A., Eigenberger, G., 1994. Gas–liquid flow in bubble columns and loop reactors: part i. detailed modeling and numerical simulation. Chemical Engineering Science 49 (24B), 5735–5746.

Veerlan, P., Tramper, J., 1987. Hydrodynamics, axial dispersion and gas–liquid oxygen transfer in an airlift bioreactor with three-phase flow. Proceedings of International Conference on Bioreactors and Biotransformations, Gleneagles, UK, Paper I4, pp. 363–373.

Wang, T.F., Wang, J.F., Zhao, B., Ren, F., Jin, Y., 2004. Local hydrodynamics in an external loop airlift slurry reactor with and without a resistance-regulating element. Chemical Engineering Communications 191, 1024–1042.